PICOSECOND PUMP-PROBE SPECTROSCOPIC STUDY OF ELECTRONIC ENERGY RELAXATION IN H-AGGREGATES OF 1,1'-DIETHYL-2,2'-DICARBOCYANINE (DDC) ON COLLOIDAL SILICA

by

SUN-YUNG CHEN, B.S.

A THESIS

IN

PHYSICS

Submitted to the Graduate Faculty
of Texas Tech University in
Partial Fulfillment of
the Requirements for
the Degree of

MASTER OF SCIENCE

Approved

Accepted

December, 1988

ACKNOWLEDGMENTS

I am deeply indebted to my research advisor, Dr. Quitevis, for his support, motivation and encouragement throughout my graduate career at Texas Tech University. I also would like to thank the other members of my committee, Dr. Borst and Dr. Menzel, for their time and help. I wish to give my special thanks to Dr. Robinson for letting us use the Picosecond and Quantum Radiation Laboratory so that we could set up and carry out the experiment. I am pleased to acknowledge the support from the Robert A. Welch Foundation and the Teaching Assistantship of the Physics Department at Texas Tech University.

Finally, I wish to dedicate this work to my parents for their love, trust and financial support.

TABLE OF CONTENTS

ACKNOWLEDGMENTS ii

ABSTRACT iv

LIST OF TABLES v

LIST OF FIGURES vi

CHAPTER

I. INTRODUCTION 1

II. EXPERIMENTAL SECTION 13

Sample Preparation 13

Picosecond Pump-probe Spectroscopy 14

Data Analysis. 22

III. EXPERIMENTAL DATA AND RESULTS 32

IV. DISCUSSION 46

V. CONCLUSION 51

REFERENCES 53

ABSTRACT

Polarized transient bleaching measurements of H-aggregates of 1,1'-Diethyl-2.2'-Dicarbocyanine (DDC) on colloidal silica were performed using picosecond time-resolved pump-probe spectroscopy. The aggregates were nonfluorescent but exhibited a broad absorption band, between 550 and 600 nm, which was blue-shifted from the monomer band at 711 nm. These spectral properties are consistent with the simple theory for one-dimensional excitons. The transient bleaching signals can be fitted well by a stretched exponential function. The nonexponential signals are attributed to a distribution of aggregates with different lifetimes, with the most probable lifetime being equal to 120-130 ps. The absorption anisotropy was constant and equal to 0.30 ± 0.04. The anisotropy is discussed in terms of the coherence properties of excitons.

LIST OF TABLES

1.1 The transition moment integrals for fluorescence emission as a function of tilt angle 12

3.1 Comparison of the fitting parameters for the polarized transient bleaching signals in Figure 3.3 39

LIST OF FIGURES

1.1 Structure of 1,1'-Diethyl-2,2'-Dicarbocyanine iodide 10

1.2 Spectral shifts of dimers and aggregates as a function of the tilt angle at constant center separation 11

2.1 Experimental set-up of the pump-probe experiment . . . 26

2.2 Interferometric arrangements for pulse autocorrelation measurements by SHG 28

2.3 Autocorrelation trace of the laser pulse 30

2.4 Typical transient bleaching signal with the apparent coherence spike 31

3.1 Absorption spectra of 20 μM DDC in (-) ethanol, (▲) water, and (+) 3.75% colloidal silica. The extinction coefficient is in units of M^{-1} cm^{-1} 36

3.2 Absorption spectra of 20 μM DDC in (+) 0.94%, (▲) 3.75% and (x) 13.5% colloidal silica 37

3.3 Typical transient bleaching signals for 20 μM DDC in 3.75% colloidal silica at 570 nm with the polarization of the probe beam parallel (top curve), 54.7° (middle curve), and perpendicular (bottom curve) to the polarization of the pump beam. 38

3.4 The normalized magic angle transient bleaching signal for 20 μM DDC in 3.75% colloidal silica (dotted curve) and pulse autocorrelation trace with FWHM of 10 ps (solid curve) 40

3.5 Time-resolved absorption anisotropy 41

3.6 Semi-logarithmic plot of the transient signal for magic angle configuration 42

3.7 The antisymmetrized transient bleaching signals for 20 μM DDC in 3.75% colloidal silica for magic angle configuration. Solid curve is the convolution of the pulse autocorrelation with an optimized antisymmetrized biexponential function. 43

3.8 The antisymmetrized transient bleaching signals for 20 μM DDC in 3.75% colloidal silica for magic angle configuration. Solid curve is the convolution of the pulse autocorrelation with an optimized antisymmetrized stretched exponential function. 44

3.9 The antisymmetrized transient bleaching signals for 20 μM DDC in 3.75% colloidal silica for magic angle configuration. Solid curve is the convolution of the pulse autocorrelation with an optimized antisymmetrized function $R_i(t) = \exp[-(t/21.1\ ps)^{1/2}]$, $\chi^2 = 3.39 \times 10^{-3}$. Inset is a residual plot between 0 and +160 ps. 45

CHAPTER I

INTRODUCTION

Many elementary physical processes in chemistry and biology occur on a picosecond time scale. The advent of picosecond optical spectroscopy makes the observation of those processes possible.[1] Picosecond optical spectroscopy utilizes the ultrashort optical pulses generated by mode-locked lasers to excite and probe rapid processes in a wide variety of materials. It has proven to be very useful and powerful in solid state physics, electronics, optics, and has the most widespread applications in chemistry and biology. [2]

The transport of electronic excitation among a set of identical molecules distributed in a medium such as a solution, glass, or mixed crystal has been a challenging problem for both the theorist and experimentalist for over 30 years.[3] With the advent of picosecond optical spectroscopy, studies of electronic energy transfer in surface-adsorbed dyes have gained much interest in recent years.[4-6] The understanding of this problem has had important applications in several areas of research such as sensitized fluorescence,[4] sensitized photochemistry,[7] solar energy collection,[6] and especially in the study of exciton propagation in photosynthetic units.[8]

The objective of this thesis is to investigate the electronic energy transport in molecular aggregates and to determine the nature of excitonic motion in these aggregates. The model systems in the present study are the cyanine dye aggregates. Understanding the

electronic excitation transport in molecular aggregates is the first step in understanding more complex biological system. The cyanine dyes have been widely used as Q-switch and mode-locking dyes in ruby laser system.[9,10] They are a remarkable class of strong light absorbers, having both sharp absorption bands and large dipole strengths. They can form aggregates in aqueous solution at high concentrations and on surfaces.[11-13] Because of the aggregation properties of cyanine dyes, they have been used as spectral sensitizers of semiconductor electrodes and silver halide emulsion.[14] The strong coupling between the molecules in these aggregates produces a new absorption band which is either red-shifted or blue-shifted from the monomer band. J-aggregates of 1,1'-diethyl-2,2'-cyanine (pseudoisocyanine, PIC) had been studied extensively.[12,15] Their spectrum exhibits a narrow absorption band, called the J-band, at about 570 nm, which is red-shifted from the monomer band at 523 nm. H-aggregates of carbocyanine dyes are another interesting system of aggregation. These aggregates give rise to the H-band, which is blue-shifted (hypsochromic) from the monomer band.[12,13] H-aggregates are thought to be different from J-aggregates in the arrangement of the monomer units. The J-aggregates state are believed to assume a head-to-tail alignment and H-aggregates state are parallel "card-pack" arrangement. These geometries and spectral shifts are plausibly predicted by the theory of molecular excitons proposed by McRae and Kasha.[16]

The cyanine dye in this study is 1,1'-diethyl-2,2'-dicarbocyanine (DDC), a photographic sensitizer (see Figure 1.1). The electronic

structure of this large conjugated molecule can be described by general quantum theory. The filled ground states contain σ, π orbitals, and lone-pair (n) electrons. Antibonding orbitals are typically π* and σ*. The possible electronic transitions in the visible and infrared spectral regions are π -> π* and n -> π* respectively, but the latter have low extinction bands and can be obscured by the strong π -> π* transitions which are characterized by the loosely bound π electrons. For such conjugated dyes, π electrons are along the methine chain which connects two heterocyclic ring systems (quinoline rings). This π electron system can be considered as free electrons moving in a one-dimensional box. Thus, the longer the chain is, the smaller the electronic energy spacing will be. The absorption spectra of these dyes are well predicted by this free-electron model. The absorption maxima are red-shifted for longer chain dyes.[17]

The cyanine dyes can form very tightly bound aggregates and exhibit spectral shifts. These aggregates may be observed on the surface of silver halide crystals, "free-standing" in solution, or adsorbed on polymetric substrates.[11] The spectral blue-shifted aggregates are designated as H-aggregates ("H" for hypsochromic) and red-shifted aggregates are called J-aggregates (probably "J" for Jelley, one of the first workers to investigate these shifts).[15] H-aggregates exhibit usually larger half-band widths than monomer and J-aggregates in contrast to this, have a sharper band. The H-aggregates of cyanine dyes can also be readily seen in aqueous solution at relatively high concentrations. They have been well

studied by W. West and coworkers.[18] The high dielectric constant of water reduces the repulsive force between the similarly charged dye cations in the aggregates. The absence of aggregation in organic solvents is attributed to the high degree of solvation. The geometry of H-aggregates of cyanine dyes has been studied not only spectroscopically, but by electron microscopy, optical microscopy, and X-ray diffraction.[11] On the basis of these studies, a deck-of-cards structure has been proposed, with the long axes of molecules perpendicular to the axis of the aggregates.

The large spectral shifts and the singlet band widths of aggregates can be explained by a one-dimensional molecular exciton model. It is simplest to consider the case of two interacting monomers (a dimer of interacting monomers). Suppose the monomers of a dimer are close enough in space to interact electronically, but the interactions are weak enough so that the individual monomers retain their identities. That is, electrons still are localized either on one monomer or on the other, but each monomer is perturbed by the electric field of the other. Each of the identical, interacting monomers is represented theoretically as a spatial distribution of oscillating electric charge. The leading term in the electronic interaction between them will be a dipole-dipole interaction.

$$J = (\mathbf{m}_1 \cdot \mathbf{m}_2)\mathbf{R}_{12}^{-3} - 3(\mathbf{m}_1 \cdot \mathbf{R}_{12})(\mathbf{m}_2 \cdot \mathbf{R}_{12})\mathbf{R}_{12}^{-5} \qquad (1.1)$$

where $\mathbf{m}_1$ and $\mathbf{m}_2$ are the dipole operators of monomer 1 and 2, respectively, and $\mathbf{R}_{12}$ is the distance between the two monomers. If this is solved quantum mechanically by considering only the ground state and the first excited state, the first order perturbation can be obtained with energy splitting of the excited state. In the point dipole approximation, the frequency splitting is [8,11]

$$\Delta\nu \text{ (dimer)} = h^{-1}(\langle m^2\rangle/r^3)(\cos\alpha - 3\cos\theta_1\cos\theta_2) \qquad (1.2)$$

where $\Delta\nu$ is the spectral shift from monomer absorption, h is Planck's constant, r is the separation of molecular centers, α is the angle between the two dipoles, and θ's are the angles between each dipole and the line joining them. $\langle m^2\rangle$, the transition dipole moment of monomer, equals $9.185 \times 10^{-39}\int_{\lambda_1}^{\lambda_2}\varepsilon(d\lambda/\lambda)$. ε is the molar extinction coefficient in $(\text{moles/L})^{-1}\ \text{cm}^{-1}$, λ is the wavelength, and λ_1, λ_2 are the limits of the well-defined absorption band. The intensities of the two split dimer bands can be written in terms of observed monomer spectral properties. The ratio of these two dipole strengths is[21]

$$\langle m^2_+\rangle / \langle m^2_-\rangle = \cot^2(\alpha/2). \qquad (1.3)$$

For parallel dipoles ($\alpha = 0°$) each perpendicular to the line joining them (H-dimer, $\theta_1 = \theta_2 = 90°$), all the strength in the (+) state. Therefore, the absorption band undergoes an excitonic blue shift.

For the molecular crystals or aggregates with more than two exciton-coupled monomers, the mathematics is more complicated,

but the theory is still straightforward. A simpler one-dimensional exciton model approach can be made by only considering the dipole-dipole interactions of the nearest neighbors and neglecting exciton-phonon coupling. The detailed quantum mechanical derivation[21,23-25] is not covered here. That derivation predicts the N-fold degenerate excited states of the N dye molecules in an aggregate are split into a band of N separated sublevels. The transition intensity is also dependent on the geometry. The predicted spectral separation of the N-mer allowed transition from the monomer band is given as follow (assuming all dipoles are parallel to each other):

$$\Delta\nu \text{ (N-mer)} = 2h^{-1}((N-1)/N)(\langle m^2\rangle/r^3)(1-3\cos^2\theta) \qquad (1.4)$$

where N is the degree of polymerization of the aggregate in question and all other symbols are as in equation 1.2 and the transition moment integrals are given in Table 1.1 as a function of the inclined angle θ. The relative energies for allowed and forbidden transitions in these aggregates are depicted in Figure 1.2 as a function of the angle of dipole-dipole interactions of the molecules in an aggregate. J-aggregates exhibit highly allowed transitions between the ground state and the first excited singlet state. Fluorescence from this state is generally strong. On the other hand, H-dimers and higher H-aggregates exhibit weak transitions between the ground state and first excited singlet state, and the more allowed transitions of H-aggregates involve higher excited-singlet states. Excitation into these latter absorption bands produces a weak fluorescence and a

relatively efficient phosphorescence. These predictions are very consistent with the fact that the J-aggregates fluoresce strongly, but the H-aggregates have very weak fluorescence. Although these point-dipole approximations are of doubtful validity in the dye under study (with long molecular length), they do predict the spectral properties of DDC semiquantitatively.

Generally, the electronic excitation (exciton) in molecular aggregates can be either a coherent delocalized combination of states or a localized excitation which hops from site to site.[22] The coherence of excitons depends on the strength of dipolar coupling between molecules and the exciton-phonon interaction.[20] Since the electronic energy states of H-aggregates of DDC can be theoretically predicted by exciton theory, the electronic energy relaxation mechanism of H-aggregates of DDC should be related to the motion of exciton. In the strong coupling case, the exciton state causes a large spectral shift. If the dipolar coupling is much larger than the exciton-phonon interaction, the coherence can readily be maintained. The excitation will be delocalized within the whole aggregate. Oppositely, if the exciton-phonon interaction is larger than the dipolar interaction, the excitation is localized on a molecule and hops from molecule to molecule.

The recent theoretical approaches set the description of exciton motion on a different basis. Immediately following the creation of exciton, the exciton is wavelike (coherent), and after a certain short period of time it becomes hopping (incoherent). Theorists differ as to the time scale on which coherence is lost.[20,22] But, the newer theories

also confirm that, for dipole-dipole interactions, the Forster description of exciton motion is the correct one once coherence is lost.[26]

This thesis is the first picosecond time-resolved spectroscopic study of the electronic energy relaxation in H-aggregates of cyanine dyes. DDC was chosen for our study, because its H-band lies within the wavelength range of our picosecond laser. We recently reported the picosecond spectroscopic study of J-aggregates of PIC adsorbed on colloidal silica.[27] The non-exponential transient bleaching signal was explained by a distribution of J-aggregates with different lifetimes. Colloidal silica was used because there is no surface-enhanced optical effect[28] or electron transfer between adsorbed molecules and the colloid.[29] Thus the system can be simplified to concentrate on the electronic energy relaxation of dye-aggregates itself. Other benefits include the small particle dimensions(50-500 A), which minimizes light scattering, the large surface-to-volume ratio, which enhance the optical detectability of surface interactions, and their ease of preparation and commercially availablity. At pH > 6, the surface silanol groups are ionized.[30] Thus the cationic dye molecules will bind readily to these negatively charged groups. However, these surface-bound molecules tend to aggregate.[31] This advantage is helpful in studying the dye aggregates on surfaces.

The application of time-resolved picosecond pump-probe techniques to study electronic energy relaxation in this system can yield a considerable amount of information that could not be available from more conventional physical/chemical techniques.

Because of the very weak fluorescence but strong absorption of H-aggregates, the pump-probe techniques is the most appropriate experimental method. Chapter 2 is devoted to describing methods of picosecond pump-probe spectroscopy and methods of data analysis in these studies. Experimental results, including sample-preparation, the steady-state spectra, and the ground state recovery signals, are also presented in chapter 3. Finally, chapters 4 and 5 are the discussion and conclusion sections. The transient photobleaching signals obtained in the system were non-exponential. The absorption anisotropy was obtained from signals with probe beam polarized parallel and perpendicular to the polarization of pump beam. The constant anisotropy is discussed in terms of the coherence of the excitons in these aggregates. Model functions were used to fit the signals to test various energy transfer mechanisms. The result can be well interpreted by a distribution of aggregates, each of which decays coherently with a different lifetime. Further experiments are proposed in order to obtain a deeper understanding of the exact energy transfer mechanism in these systems.

DDC

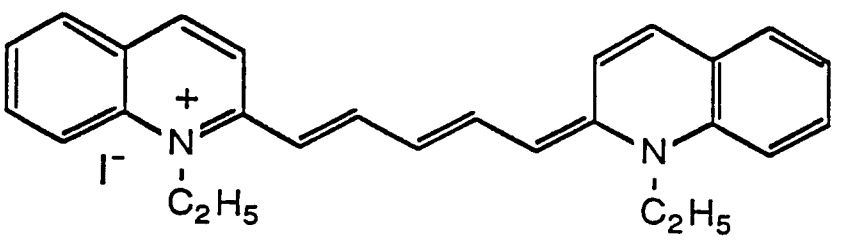

Figure 1.1

Structure of 1,1'-Diethyl-2,2'-Dicarbocyanine iodide

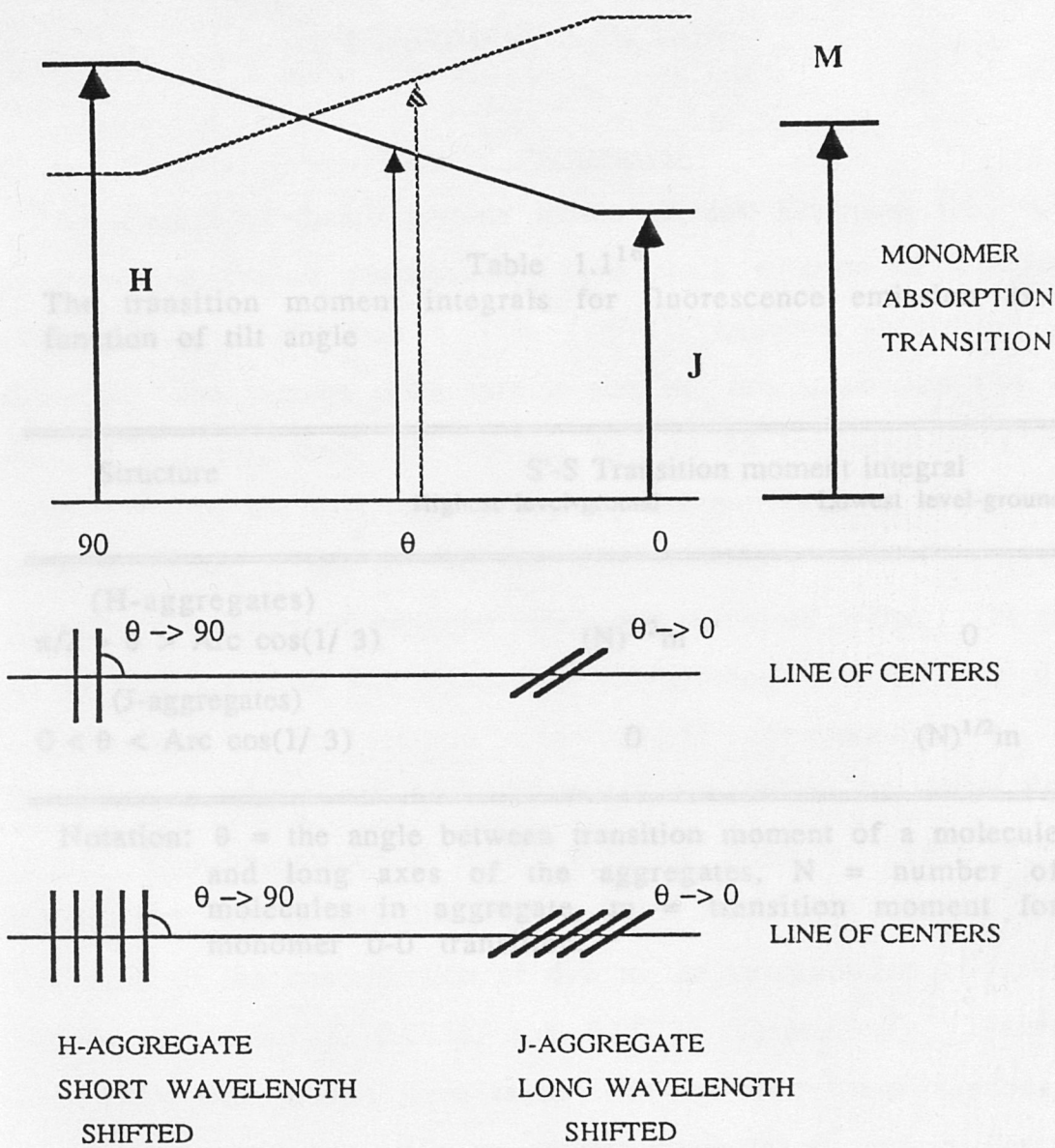

Figure 1.2
Spectral shifts of dimers and aggregates as a function of the tilt angle at constant center separation

Table 1.1[16]

The transition moment integrals for fluorescence emission as a function of tilt angle

Structure	S'-S Transition moment integral	
	Highest level-ground	Lowest level-ground
(H-aggregates) $\pi/2 > \theta >$ Arc cos(1/ 3)	$(N)^{1/2}m$	0
(J-aggregates) $0 < \theta <$ Arc cos(1/ 3)	0	$(N)^{1/2}m$

Notation: θ = the angle between transition moment of a molecule and long axes of the aggregates, N = number of molecules in aggregate, m = transition moment for monomer 0-0 transition.

CHAPTER II

EXPERIMENTAL SECTION

Sample Preparation

1,1'-diethyl-2,2'-dicarbocyanine iodide (Kodak Chemical Co.) was used without further purification. The stock solution of colloidal silica (Nalco 1115) was a 15% (wt/vol) aqueous suspension at pH=10.4. The average silica particle size in this suspension was 40 Å. At this pH, there are between 60 and 65 ionization sites per colloid.[32] 10 mL samples with various concentrations of silica were made by diluting 1 mL of a 200 μM ethanol solution of DDC with the appropriate volumes of colloidal silica and deionized water. The pH of the final solutions was adjusted by the addition of KOH. The dye concentration in the samples was 20 μM corresponding to an maximum absorbance of 0.1 ~ 0.2 in a 1 mm cell in the visible light range. This absorbance is in the optimum response range of the spectrometer. For 20 μM DDC in 0.94, 3.75, and 13.5 % colloidal silica, the ratios of the concentration of dye to the concentration of colloid particles were 0.103, 0.0258, and 0.00727, respectively. Steady-state absorption spectra were taken with a Perkin-Elmer Lambda 4 spectrometer, and the emission spectra were taken with a Perkin-Elmer MPF-44B spectrofluorimeter. Spectra were digitized and input to a DEC VAX 11/730 minicomputer for numerical integration and plotting. The samples were spun in a Beckman L7-65 Ultracentrifuge

at 20K rpm (~64,000 g) for 14 hrs. Spectrophotometry of the supernatant revealed all the dye was adsorbed on the silica particles.

Picosecond Pump-probe Spectroscopy

Introduction

The picosecond pump-probe technique we used is the so called "ground state recovery" (GSR). Because this method utilizes absorption rather than fluorescence for detection, non-radiating molecular systems can be studied. The idea of "ground state recovery" is as follow: the first pulse (pump pulse) bleaches the ground state population to the excited state and the second weaker, delayed pulse (probe pulse) monitors the return of the excited state population by absorption at the same wavelength. The measured signal is the change in transmission of the probe pulse through the sample as a function of time delay after the excitation by pump pulse. Stimulated emission of the excited molecules by the probe beam is assumed to be unimportant because of the fast vibrational relaxation and equilibration.[33] Thus the quantity of interest is the instantaneous absorption coefficient of the sample at time t after excitation.

If linearly polarized light is used, this absorption coefficient will not only depend on the recovery of ground state population, but also the relative polarization of the pump and probe beams. The probability for absorption of a photon depends on the angle between the polarization of the light and the transition dipole moment of the molecule. Therefore, excitation of a random sample with polarized

light produces an anisotropic angular distribution of excited dipoles: those dipoles that are aligned more closely with the electric vector have a higher probability of being excited: this is the principle called photoselection. The corresponding anisotropy in the ground state population induces a dichroism. The absorption coefficient for light polarized parallel to the excitation polarization is smaller, since the effective bleaching is greater in this configuration than for light polarized perpendicular to the excited pulse. Therefore, the GSR signals contain information of absorption anisotropy as well as population kinetics. That is, population kinetics is not the only contribution to the signals. Induced dichroism due to anisotropic absorption is also involved. Since rotational reorientation and energy transfer contribute to the absorption anisotropy, the kinetics of these two processes can be extracted from the decay behavior of time-resolved absorption anisotropy.

In general, the absorption coefficients for probe beam with parallel and perpendicular polarization to the pump beam polarization are given by[34]

$$\alpha_{//}(t) = \alpha_o - C(1+2r(t))\, K(t) \qquad (2.1)$$

$$\alpha_{\perp}(t) = \alpha_o - C(1- r(t))\, K(t) \qquad (2.2)$$

α_o is the normal absorption coefficient measured without pump pulse excitation, C is a constant, r(t) is absorption anisotropy, and K(t) is the excited state decay function. Since the transient bleaching signals of the ground state recovery measurements correspond to the change of

transmission as a function of time t after the sample is excited by the pump pulse, the relation between absorption coefficient and transmission change must be considered. By applying Beer's law to the probe pulse at time t after the pump pulse,

$$I(t) = I_o e^{-\alpha(t)L} \tag{2.3}$$

where I(t) is the probe pulse intensity after the sample, I_o is the intensity before the sample, $\alpha(t)$ the absorption coefficient of the sample after time t, and L the sample width. $\alpha(t)$ can be expressed as

$$\alpha(t) = \alpha_o + \Delta\alpha(t) \ . \tag{2.4}$$

Here $\Delta\alpha(t)$ is the absorption coefficient change due to bleaching. Substituting these expressions into Beer's law, one gets for probe transmission at time t

$$T(t) = I_o e^{-\alpha_o L} e^{-\Delta\alpha(t)} = T_0 e^{-\Delta\alpha(t)L} \tag{2.5}$$

T_0 is the transmission in the absence of bleaching. When $\Delta\alpha(t)$ is small, as is usually the case in practice, the exponential can be expanded. Equation 2.5, then becomes

$$T(t) = T_0(1-\Delta\alpha(t)L) \ . \tag{2.6}$$

Thus,

$$\Delta T(t) = T(t) - T_0 = - T_0 \Delta\alpha(t) L \ . \qquad (2.7)$$

By substituting equations 2.1, 2.2, 2.4 into equation 2.7, one sees that the signals which correspond to the change of transmission for the parallel and perpendicular polarizations are given by

$$S_{//}(t) = \Delta T_{//}(t) = T_0 CL(1+2r(t))\, K(t) \qquad (2.8)$$

$$S_{\perp}(t) = \Delta T_{\perp}(t) = T_0 CL(1 - r(t))\, K(t) \ . \qquad (2.9)$$

We then form the sum $S_{//}(t) + 2S_{\perp}(t)$,

$$S_{//}(t) + 2S_{\perp}(t) = 3T_0\, CLK(t) \qquad (2.10)$$

which depends on population kinetics only. For a probe direction specified by an angle θ to the parallel direction, the measured transmission change is

$$S_{\theta}(t) = \cos^2\theta S_{//}(t) + \sin^2\theta S_{\perp}(t) \ . \qquad (2.11)$$

The condition which leads to the linear combination in equation 2.9 is $\tan^2\theta=2$, i.e., $\theta=54.7°$ which is known as the "magic angle." Therefore, if it is desired to record level kinetics without any contribution from orientational relaxation, the probe beam should have a polarization of 54.7° with respect to that of the pump beam.

$$S_{54.7^0}(t) = [S_{//}(t) + 2S_{\perp}(t)]/3 = T_0\, CLK(t) \qquad (2.12)$$

Similarly, if the difference

$$S_{//}(t) - S_{\perp}(t) = 3T_0 CLr(t)K(t) \qquad (2.13)$$

is taken, the time-resolved absorption anisotropy r(t) can be calculated by

$$r(t) = [S_{//}(t) - S_{\perp}(t)] / [S_{//}(t) + 2S_{\perp}(t)] \quad . \qquad (2.14)$$

From the decay behavior of r(t), the rotational relaxation and energy transfer can be elucidated.[35-37]

Experimental Arrangement

The setup of our pump-probe apparatus is shown in Figure 2.1. The picosecond pulse-train was generated by a synchronously pumped rhodamine 6G dye laser system: A Coherent Radiation, Inc. argon-ion laser (CR-12) was mode-locked at 38.219 MHz, the 514.5 nm plasma line being used to pump a Coherent 700 dye laser containing rhodamine 6G. The generated train of pulses has a 8-10 ps FWHM at 76 MHz repetition rate and an average power of 75 mW at 570 nm. The dye laser can be tuned from 560-618 nm. 570, 580, 590, and 600 nm were used in this experiment for the absorption maxima of the H-bands for systems with different concentrations. The laser beam was split into a pump beam and a probe beam by a pellicle beam splitter (BS1) with a reflectivity of 8%. Thus about 92%

of the intensity was used to excite the sample and 8% was used as probe beam.

The probe beam was directed into two mirrors mounted on a computer-controlled translation stage, and a variable delay can be set. The probe pulse delay corresponded to 2.0 ps/step. The pump beam was incident on a Matsushita ELF-M120 acoustooptic modulator (AOM) operating with modulation depth of 60-80% at 10.24 MHz. The appropriate polarization direction can be assigned by passing the pump beam through a Glan-Thompson polarizer (P1) and the probe beam through a polarization rotator (PR). The two noncollinear but parallel beams were then focused with a 10-cm focal length achromat to a common spot size of ~180 μm in a 3 mm pathlength spinning sample cell (S). (The spot size was measured by transmission measurements through calibrated pinholes.) An aperture was used so that only the probe beam can go through it and the pump beam was blocked. The transmitted probe beam passed through an interference filter at the wavelength of the laser and was detected with a photomultiplier tube (PMT).

The signals were detected at the frequency of 10.24 MHz corresponding to the induced modulation in the probe beam. The output of the PMT was fed into a EG&G 5202 MHz lock-in amplifier (LIA). The analog output of the LIA was digitized and stored in a microcomputer. Raw time-resolved bleaching signals scanned from -160 to +160 ps were transferred to a DEC VAX 11/730 minicomputer for data analysis.

The high frequency (10.24 MHz) modulation was used instead of low frequency (audio) chopping, because amplitude noise in the dye laser arises mainly from mechanical fluctuations in the dye stream and is much worse in the kilohertz than in the megahertz region.[3,4] The average incident laser powers of the pump and probe beams at the sample were 15 and 10 mW, respectively. These intensity were so low that the stimulated emission and other intensity related effects were assumed unimportant. To confirm this, an intensity study was carried out by using neutral density filters to gradually reduce the pump beam intensity. No apparent change in decay behavior was noticed in the signals. Spinning of the sample was necessary to minimize the effects of dye photooxidation and local heating.

Autocorrelation Trace

Because mode-locked cw dye laser pulses are only a few picoseconds in duration, it is impossible to measure them by conventional detectors and electronics. Thus a nonlinear optical technique has to be applied. In this technique a crystal with nonlinear electrooptical properties is used to convert a portion of the laser light from frequency ω to frequency 2ω . The intensity of the second harmonic light is measured as a function of the time delay between two replica pulses which are arranged to overlap spatially in the crystal. Various experimental arrangements for pulse autocorrelation measurements by second harmonic generation(SHG) are illustrated in Figure 2.2.[2] The measured signal is proportional to

the autocorrelation function of the pulse intensity I(t)and is given in normalized form by

$$G(\tau) = \langle I(t)\ I(t-\tau)\rangle / \langle I^2(t)\rangle \qquad (2.15)$$

where the brackets denote an average over a sufficiently long period of time. $G(\tau)$ has a maximum value of 1 at zero time delay, and decays to zero at longer delay if the intensity I(t) is a single isolated pulse. The relationship between I(t) and $G(\tau)$ depends on the functional form of I(t). The autocorrelation function of a Gaussian pulse intensity is also a Gaussian function, with a FWHM which is larger than the intensity FWHM by a factor of $\sqrt{2}$. In general, smooth pulse profiles yield smooth autocorrelation functions, with their widths related by a numerical constant between 1 and 2. Autocorrelation traces were obtained in our experiments using the noncollinear geometry. In this geometry type I phase-matching, zero background SHG is measured. By replacing the sample in the pump-probe apparatus by a potassium dihydrogen phosphate (KDP) crystal, optimum autocorrelation measurements were made by using standard chopping techniques. The probe beam was chopped at ~ 1 kHz, and the modulated SHG signal was detected with a kilohertz LIA. A typical autocorrelation trace is shown in Figure 2.3. The FWHM of the pulse autocorrelation in our laser system was 10.7 ps.

Data Analysis

The time-resolved pump-probe experiment, in principle, has excellent time resolution because the pump and probe pulses are derived by splitting the beam. Consequently, there is no time jitter between the pulses. Unfortunately, when the pump and probe pulses are derived from a common laser, it will produce a additional signal contribution around zero delay which is called the coherence coupling artifact or the coherence spike. A typical transient bleaching signal with the apparent coherence spike is shown in Figure 2.4. The narrow peak at zero delay is due to the coherent interaction of pump and probe pulses. Around zero delay the pump and probe fields interfere in the sample. In this case the probe is not just responding to population bleaching produced by the pump, but is interacting with the pump field itself. The interaction can be described as the diffraction of some of the pump pulse into the probe pulse direction by a transient population grating produced by interference of the two fields. The effect persists only while the interference occurs, and hence the width of coherence spike is related to the coherence time of the laser. Coherent-coupling effects were first observed in picosecond pump-probe experiments by Shank and Auston.[38] A general theoretical treatment has been given by Jena and Lessing.[39]

The decay of the signal can be misinterpreted if the coherent coupling artifact is not removed when fitting the data. Since the coherence spike is symmetric about zero delay, the anti-symmetrizing procedure of Engh et al.[40] can be used to eliminate the coherent coupling contribution. Briefly, for slightly noncollinear,

copropagating beams, in the small signal limit, the observed signal as a function of delay time can be written as a sum of the terms:

$$S(\tau) = \gamma(\tau) + \beta(\tau) \tag{2.16}$$

$\beta(\tau)$ is the coherent contribution to the signal and is symmetric with respect to delay. For times longer than the dephasing time, $\gamma(\tau)$ corresponds to the convolution of the molecular response with the intensity autocorrelation of the pulse

$$\gamma(\tau) = \int_{-\infty}^{\infty} G(t')\ R^i(\tau + t')\ dt' \tag{2.17}$$

$G(t')$ is the second-order autocorrelation function, which is symmetric with respect to delay time, and $R^i(t)$ is the incoherent molecular response. Forming the antisymmetrized function $S_a(t)$ removes the coherent coupling artifact:

$$S_a(\tau) = (1/2)[S(\tau)-S(-\tau)] = (1/2)[\gamma(\tau)- \gamma(-\tau)] \tag{2.18}$$

The antisymmetrized signal can also be written as

$$S_a(\tau) = \int_{-\infty}^{\infty} G(t')\ R^a(\tau + t')\ dt' \tag{2.19}$$

where $R^a(t)$ is the antisymmetrized molecular response function

$$R^a(t) = (1/2)[R^i(t)-R^i(-t)] \tag{2.20}$$

In this work, we used various model functions to represent $R^i(t)$. The single exponential function is the basic one to describe the intrinsic energy decay. The biexponential is widely used for non-exponential signals. The stretched exponential function is appropriate for systems in which there is a statistical spread of relaxation times,[41,42] such as might be the case for H-aggregates adsorbed on colloidal silica. Forster type energy transfer functions are also applied to describe the exciton migration mechanism. The biexponential function is given by

$$R^i(t) = A_1\exp(-t/\tau_1) + A_2\exp(-t/\tau_2) \quad . \tag{2.21}$$

The stretched exponential function is given by

$$R^i(t) = A\exp[(-t/\tau)^\alpha] \tag{2.22}$$

where α is related to the width of the distribution. The lifetime at the peak of the distribution can be derived by the inverse Laplace transform.[51] The Forster energy transfer function is given by

$$R^i(t) = A\exp[-C(t/\tau)^\alpha] \tag{2.23}$$

where C is the concentration of traps, τ is the hopping time and α = d/6, d is the dimension of the system.[41]

Transient bleaching signals were antisymmetrized about $\tau = 0$. The antisymmetrized signals were fit to the convolution of the pulse

autocorrelation with the antisymmetrized models. The fitting was done with a nonlinear convolute-and-compare analysis using a Marquardt algorithm which minimized the sum of the squares of the residuals (χ^2) by varying the parameters.[43] Because the weighting factor is hard to be determined in our system, the unweighted χ^2 is used.

Figure 2.1

Experimental set-up of the pump-probe experiment: AMP, fast buffer amplifier; AOM, acoustooptic modulator; A, aperature; BS, 8% reflectivity pellicle beam splitter; IF, inteference filter; ND, neutral density filter; L1 and L2, lenses; P1, crossed Glan-Thompson polarizers; PMT, photomultiplier tube; PR, polarization rotator; PS, prism; S, spinning sample; SM, stepper motor.

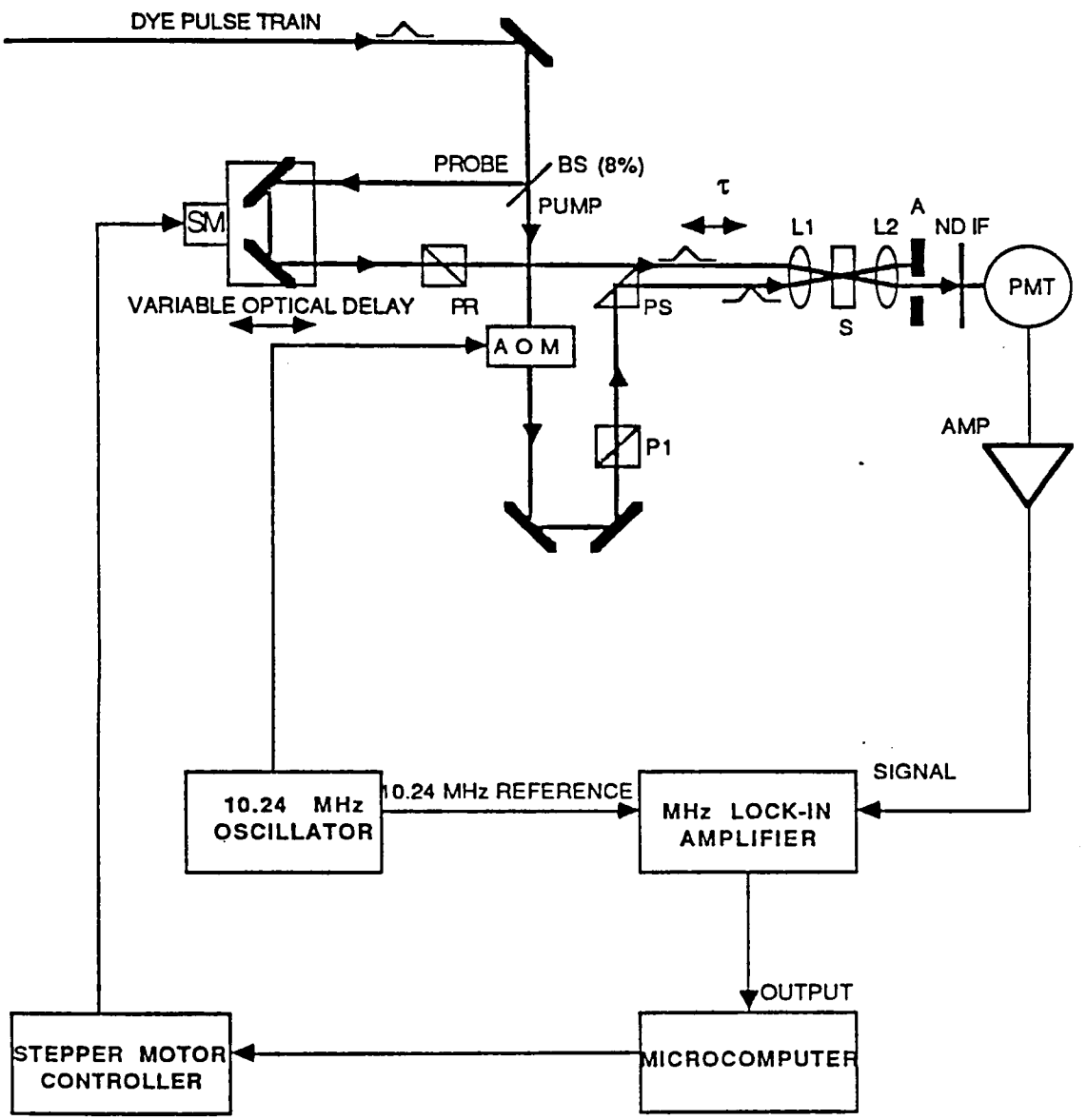
DYE PULSE TRAIN
PROBE
BS (8%)
PUMP
τ
SM
L1
L2
A
ND IF
PMT
VARIABLE OPTICAL DELAY
PR
PS
S
A O M
P1
AMP
10.24 MHz OSCILLATOR
10.24 MHz REFERENCE
MHz LOCK-IN AMPLIFIER
SIGNAL
OUTPUT
STEPPER MOTOR CONTROLLER
MICROCOMPUTER

laser pulse
variable
delay (τ)
50/50
beam splitter
lens
nonlinear
crystal
lens
photodetector
UV-transmitting
filter

(a)

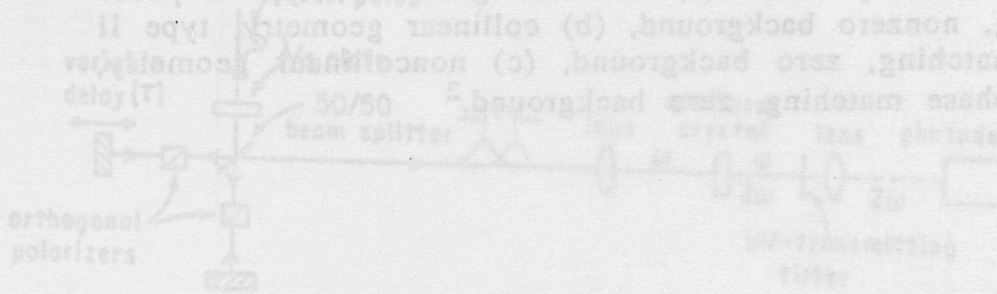
variable
delay (τ)
50/50
beam splitter
orthogonal
polarizers
UV-transmitting
filter

(b)

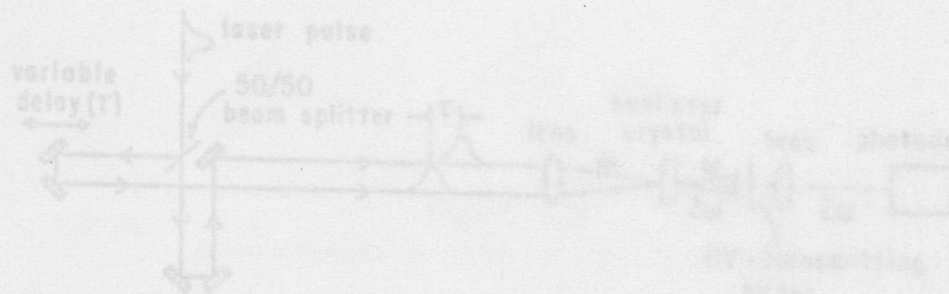
laser pulse
variable
delay (τ)
50/50
beam splitter

(c)

Figure 2.2
Interferometric arrangements for pulse autocorrelation measurements by SHG: (a) collinear geometry, type I phase matching, nonzero background, (b) collinear geometry, type II phase matching, zero background, (c) noncollinear geometry, type I phase matching, zero background.[2]

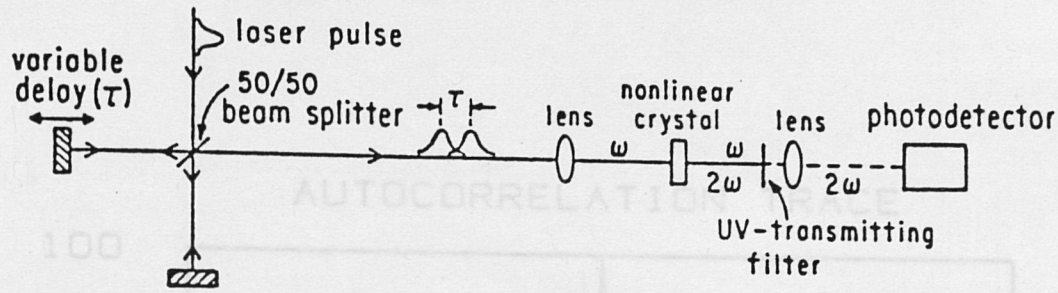
laser pulse
variable
delay (τ)
50/50
beam splitter
τ
lens
nonlinear
crystal
lens
photodetector
ω
ω
2ω
2ω
UV-transmitting
filter

(a)

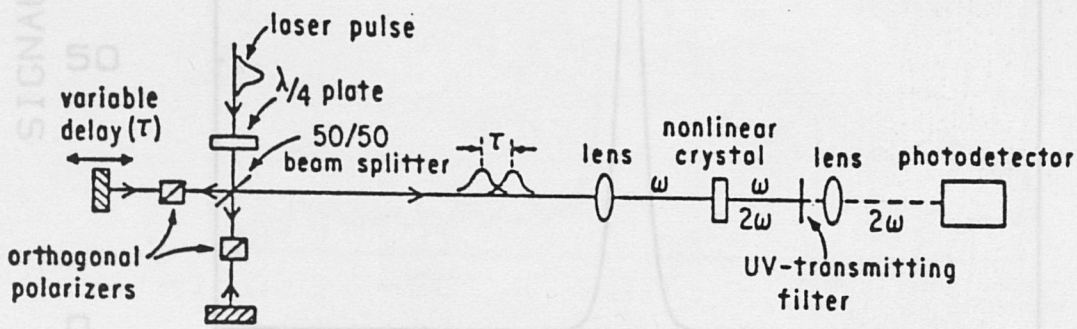
laser pulse
λ/4 plate
variable
delay (τ)
50/50
beam splitter
τ
lens
nonlinear
crystal
lens
photodetector
ω
ω
2ω
2ω
orthogonal
polarizers
UV-transmitting
filter

(b)

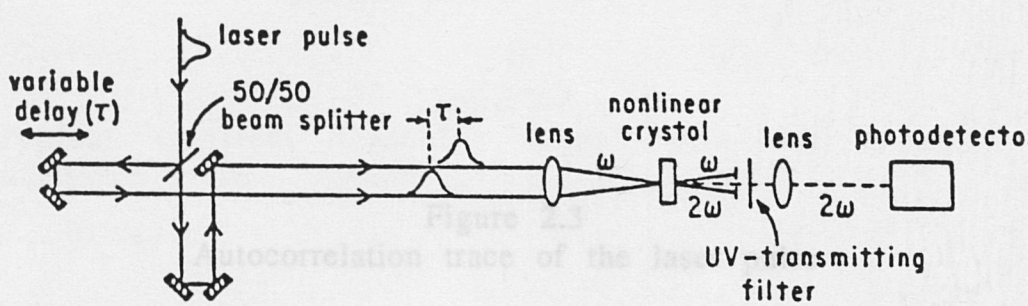
laser pulse
variable
delay (τ)
50/50
beam splitter
τ
lens
nonlinear
crystal
lens
photodetector
ω
ω
2ω
2ω
UV-transmitting
filter

(c)

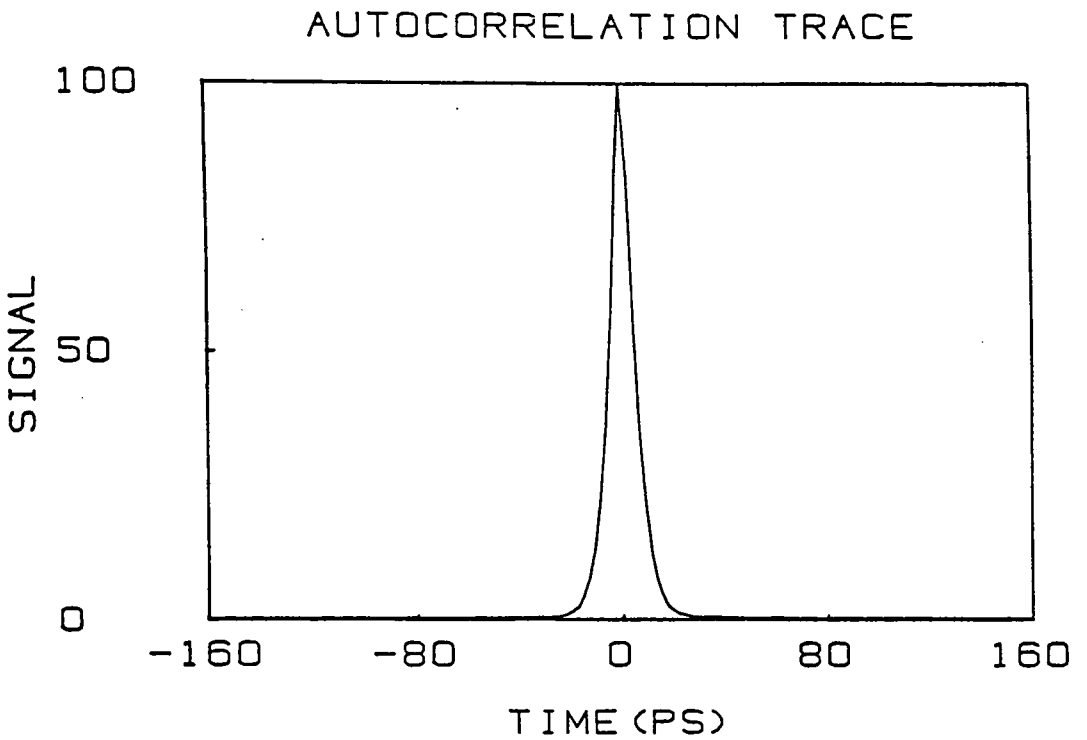

Figure 2.3
Autocorrelation trace of the laser pulse

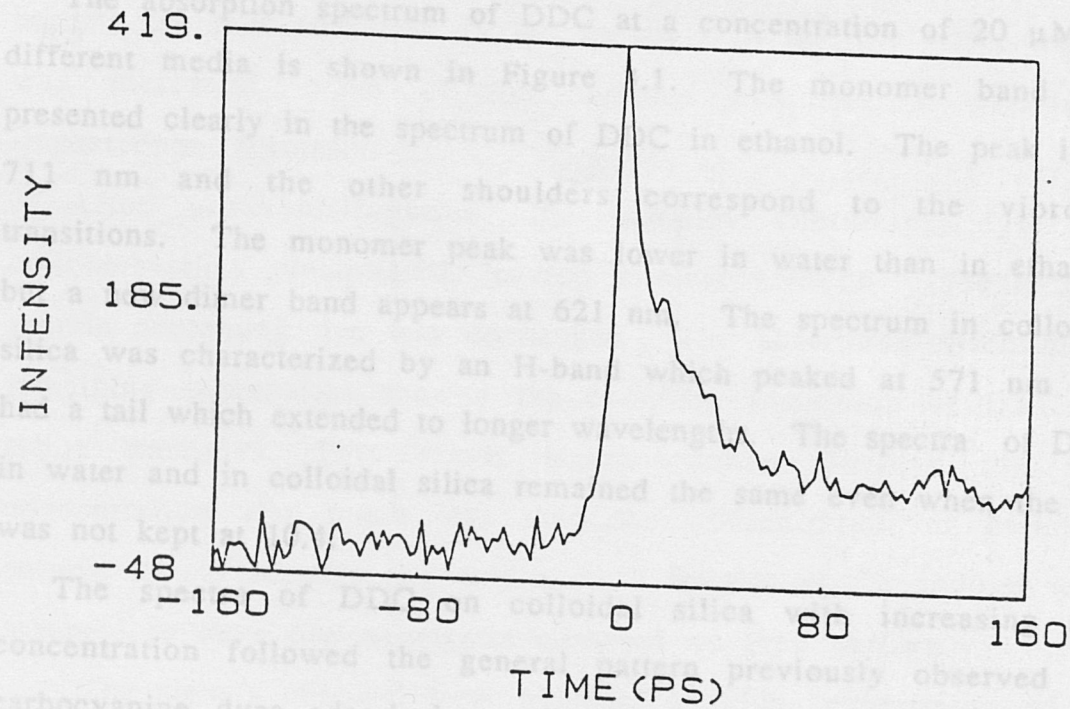

Figure 2.4
Typical transient bleaching signal with the apparent coherence spike

CHAPTER III

EXPERIMENTAL DATA AND RESULTS

The absorption spectrum of DDC at a concentration of 20 μM in different media is shown in Figure 3.1. The monomer band was presented clearly in the spectrum of DDC in ethanol. The peak is at 711 nm and the other shoulders correspond to the vibronic transitions. The monomer peak was lower in water than in ethanol, but a new dimer band appears at 621 nm. The spectrum in colloidal silica was characterized by an H-band which peaked at 571 nm and had a tail which extended to longer wavelengths. The spectra of DDC in water and in colloidal silica remained the same even when the pH was not kept at 10.4.

The spectra of DDC on colloidal silica with increasing dye concentration followed the general pattern previously observed for carbocyanine dyes adsorbed on silver halide grains in photographic emulsions.[44,45] For a fixed dye concentration of 20 μM, the H-band shifted to shorter wavelengths (593 to 558 nm) and became narrower as the colloid concentration was decreased from 13.5% to 0.94% (Figure 3.2). The blue shift of the H-band head can be explained by the formation of larger aggregate as higher concentration ratios of DDC to silica. The monomer peak at approximately 702 nm was discernable in the spectrum of the sample containing 13.5% colloidal silica, which corresponds to the

smallest DDC/silica ratio, can be attributed to adsorbed isomers of the monomer whose electronic energy levels are perturbed by the surface but not by interactions between dye molecules. The H-band became the dominant peak in the spectrum as the dye concentration was increased. None of the samples exhibited a detectable fluorescence spectrum.

After ultracentrifugation, the samples containing dye and colloidal silica precipitated, leaving a clear solution. The control sample containing dye was unchanged. The absorption spectrum of remaining supernatant showed the complete adsorption of DDC on silica particles. This result is reasonable, because the dye concentration was much less than the concentration of colloidal particle in our samples and only a small fraction of the colloids were assumed to have dye aggregates adsorbed on their surface.

The signals obtained from transient bleaching experiments of H-aggregates on colloidal silica are shown in Figure 3.3 for different polarization configurations. The risetime of the signal is limited by the pulse width. The normalized signal and autocorrelation trace are plotted together to show the relation (Figure 3.4). The signals $S_{//}$ and $S_{\perp}$, and $S_{54.7}$ for different polarization configurations(shown in Figure 3.3) had the same time-dependence (Table 3.1). The absorption anisotropy r(t) which was obtained by using equation 2.12 is shown in Figure 3.5. It almost remained constant in our study time range 0 - 160 ps. A typical signal with magic angle configuration is plotted in Figure 3.6 by semilogrithmic graph which shows the excited state population decay is nonexponential in our

system. The antisymmetrized signal can be well fitted by a biexponential function or a stretched exponential function, as indicated by the random residuals (see Figures 3.7, 3.8). The signal exhibits a dominant short component with decay time of 19 ps and a long component with a decay time of 166 ps. The presence of this short component confirms the need to use the antisymmetrization procedure to fit the data.

The stretched exponential fit of data from several runs gave α = 0.46 ± 0.02 and τ_p =17 ± 5 ps. The constant τ_p obtained from the stretched-exponential fit is roughly a quarter of the value obtained from the PIC data.[26] However, the value of α obtained for the H-aggregates of DDC and the value of α = 0.54 for the J-aggregates of pseudoisocyanine (PIC) on colloidal silica are almost equal to 1/2. The α's differ by only 8% from their average value of 0.50. A best fit of the DDC data in Figure 3.9 to an $\exp[-(t/\tau_p)^{1/2}]$ decay law is obtained with τ_p = 21 ps, which is within experimental error close to the value obtained from the stretched exponential fit for this data.

Changing the concentration from 0.94% to 13.5% and varying the excitation wavelength between 570 and 590 nm for a fixed colloid concentration had little effect on the shape of the signals.

The transient bleaching signals did not change when the pump intensity was decreased by a factor of four. Hence, there was no evidence under these experimental conditions that singlet-singlet exciton annihilation will be the major component of the isotropic decay.[45] For these pump intensities, the extinction coefficient of the

sample did not change and was equal to what we obtained with the absorption spectrometer. This implied that there were no multi-photon processes occurring under the conditions of this experiment.

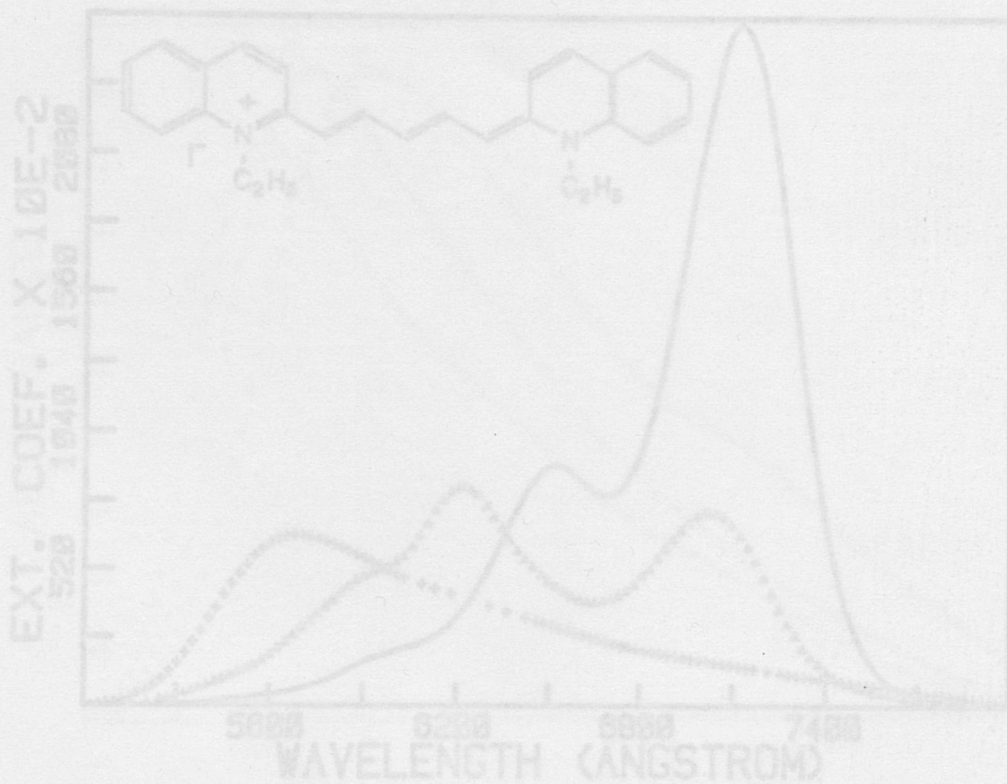

Figure 3.1
Absorption spectra of 20 μM DDC in (-) ethanol, (▲) water, and (+) 3.75% colloidal silica. The extinction coefficient is in units of M^{-1} cm^{-1}.

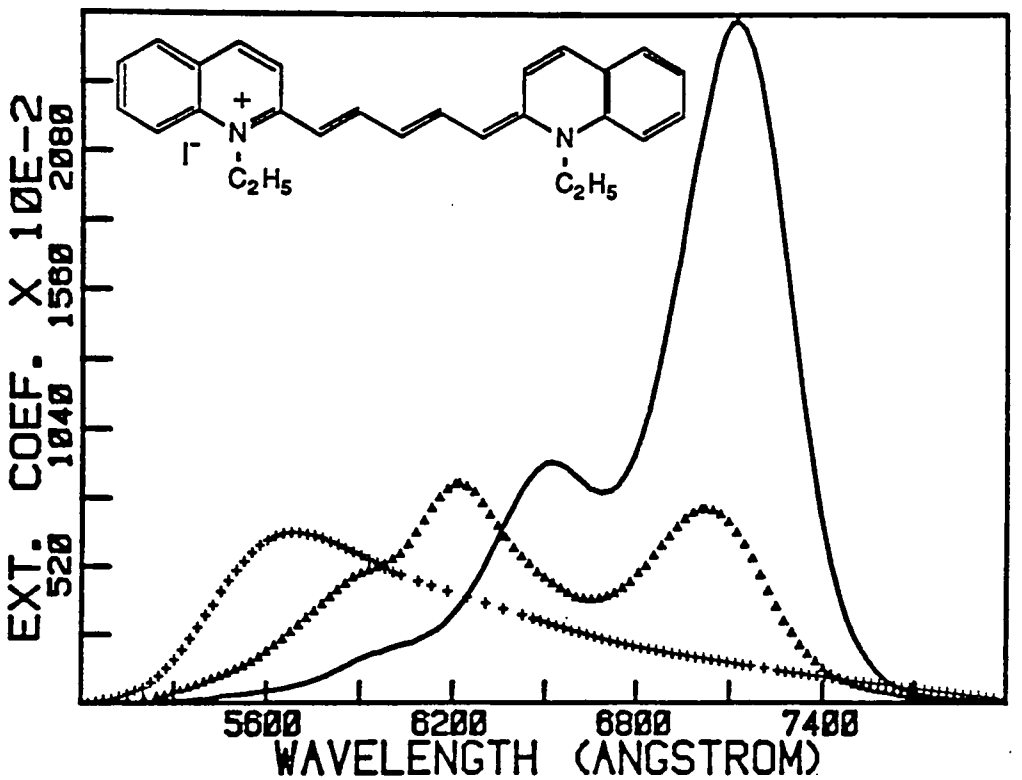

Figure 3.1

Absorption spectra of 20 μM DDC in (-) ethanol, (▲) water, and (+) 3.75% colloidal silica. The extinction coefficient is in units of M^{-1} cm^{-1}.

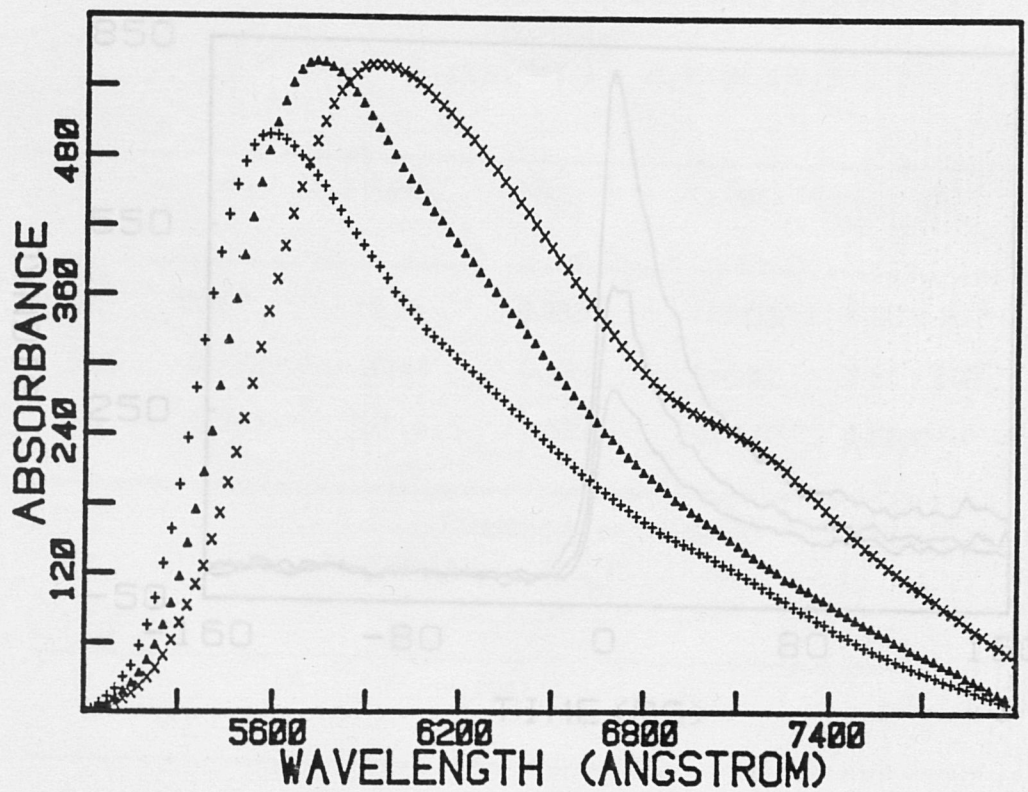

Figure 3.2
Absorption spectra of 20 μM DDC in (+) 0.94%, (▲) 3.75% and (x) 13.5% colloidal silica.

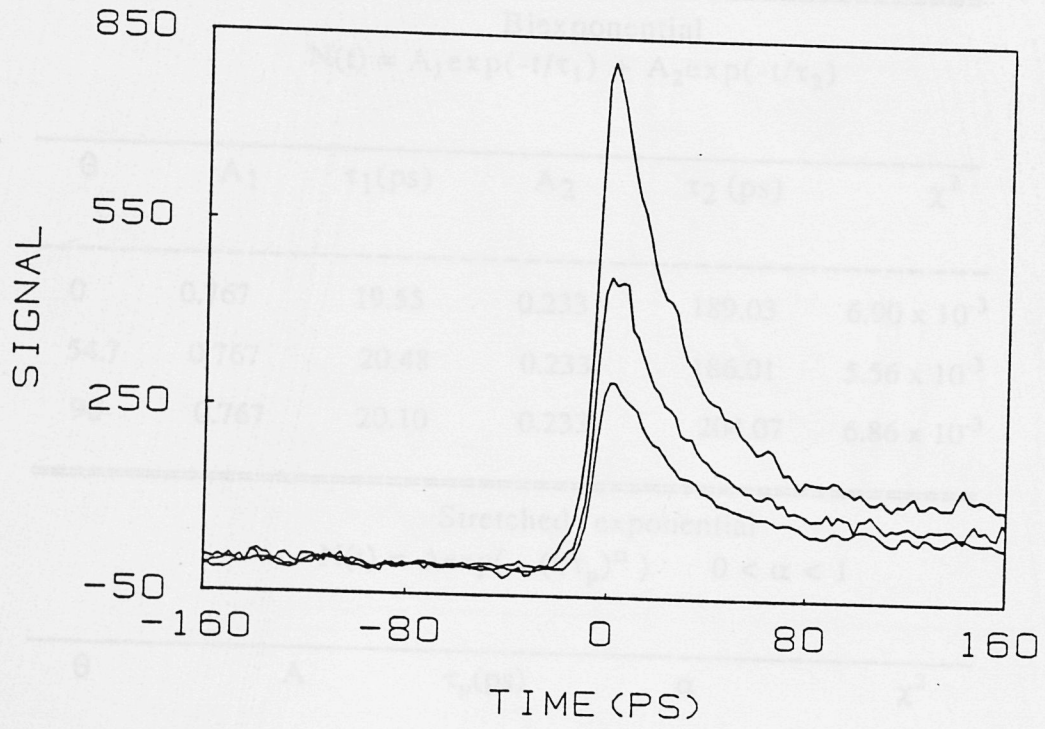

Figure 3.3

Typical transient bleaching signals for 20 μM DDC in 3.75% colloidal silica at 570 nm with the polarization of the probe beam parallel (top curve), 54.7° (middle curve), and perpendicular (bottom curve) to the polarization of the pump beam.

Table 3.1
Comparison of the fitting parameters for the polarized transient bleaching signals in Figure 3.3

Biexponential

$N(t) = A_1 \exp(-t/\tau_1) + A_2 \exp(-t/\tau_2)$

θ	A_1	τ_1(ps)	A_2	τ_2 (ps)	χ^2
0	0.767	19.55	0.233	189.03	6.90×10^{-3}
54.7	0.767	20.48	0.233	186.01	5.56×10^{-3}
90	0.767	20.10	0.233	204.07	6.86×10^{-3}

Stretched exponential

$N(t) = A\exp(- (t/\tau_p)^{\alpha}) \quad 0 < \alpha < 1$

θ	A	τ_p(ps)	α	χ^2
0	0.3796	19.6	0.4582	6.08×10^{-3}
54.7	0.3951	18.9	0.4600	5.01×10^{-3}
90	0.3785	20.3	0.4548	5.59×10^{-3}

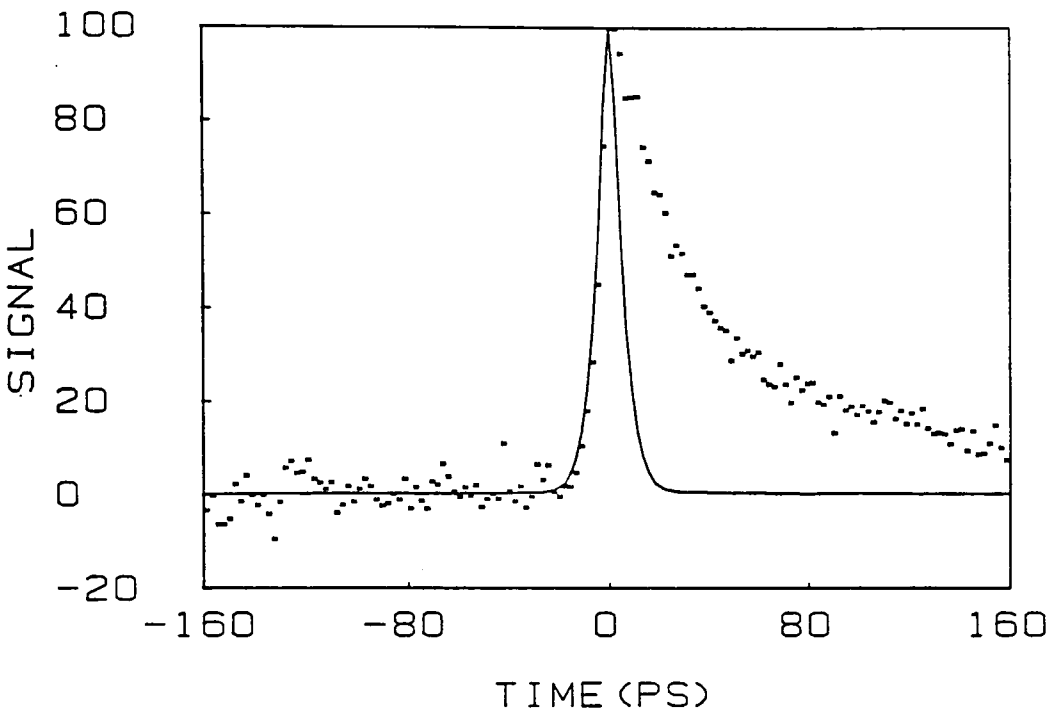

Figure 3.4
The normalized magic angle transient bleaching signal for 20 μM DDC in 3.75% colloidal silica (dotted curve) and pulse autocorrelation trace with FWHM of 10 ps (solid curve)

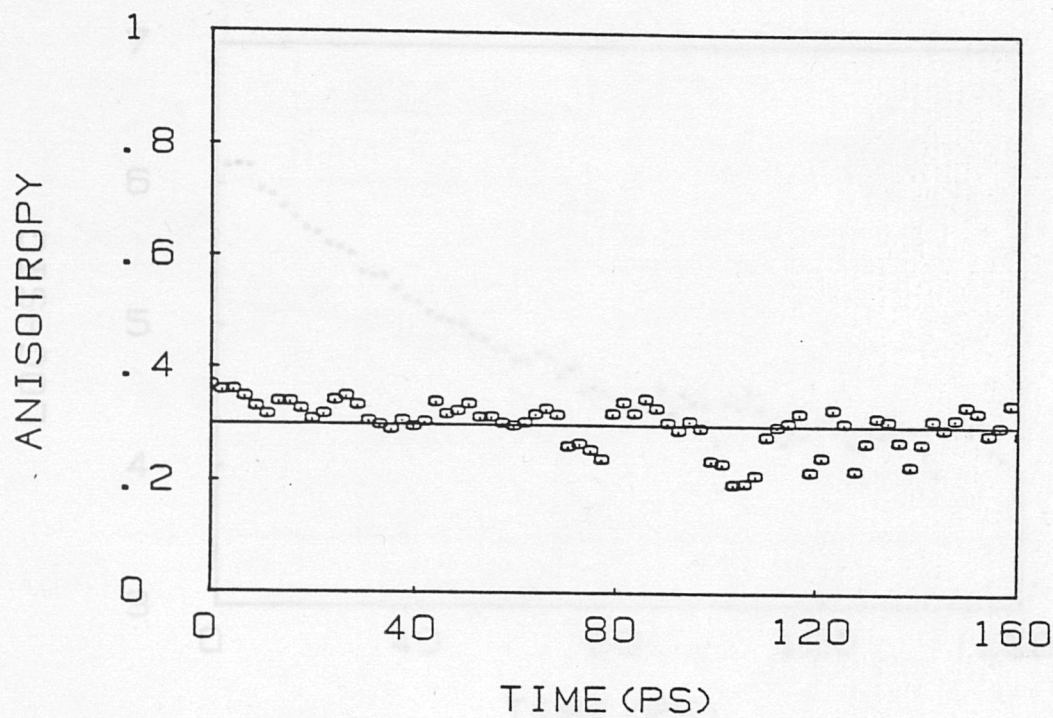

Figure 3.5
Time-resolved absorption anisotropy

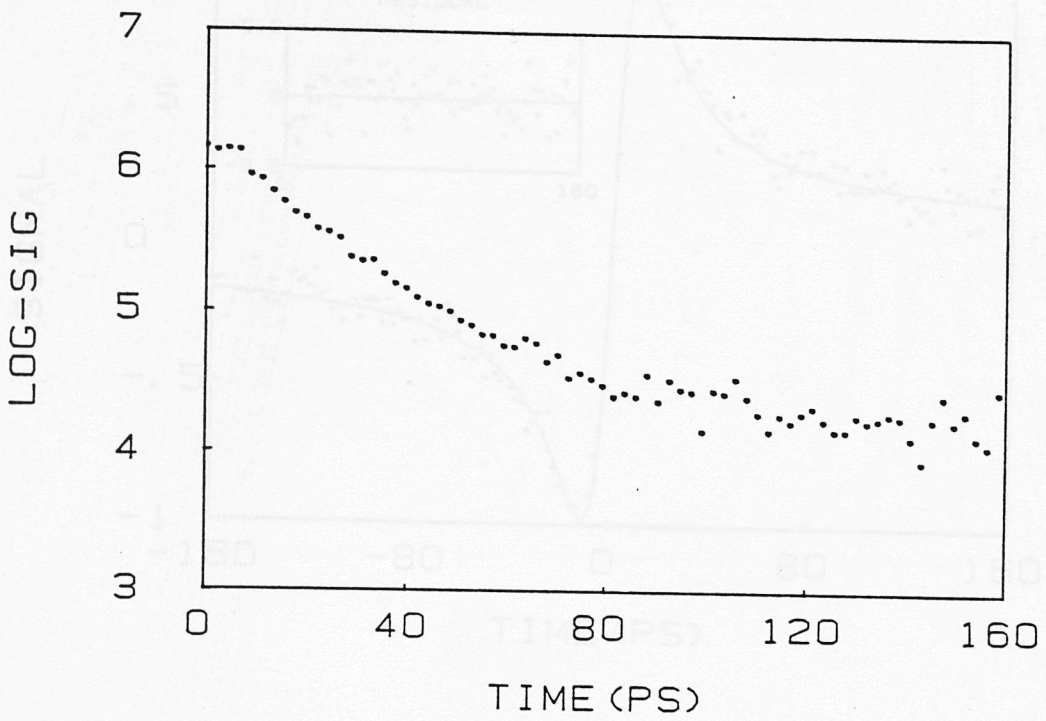

Figure 3.6
Semi-logarithmic plot of the transient signal for magic angle configuration

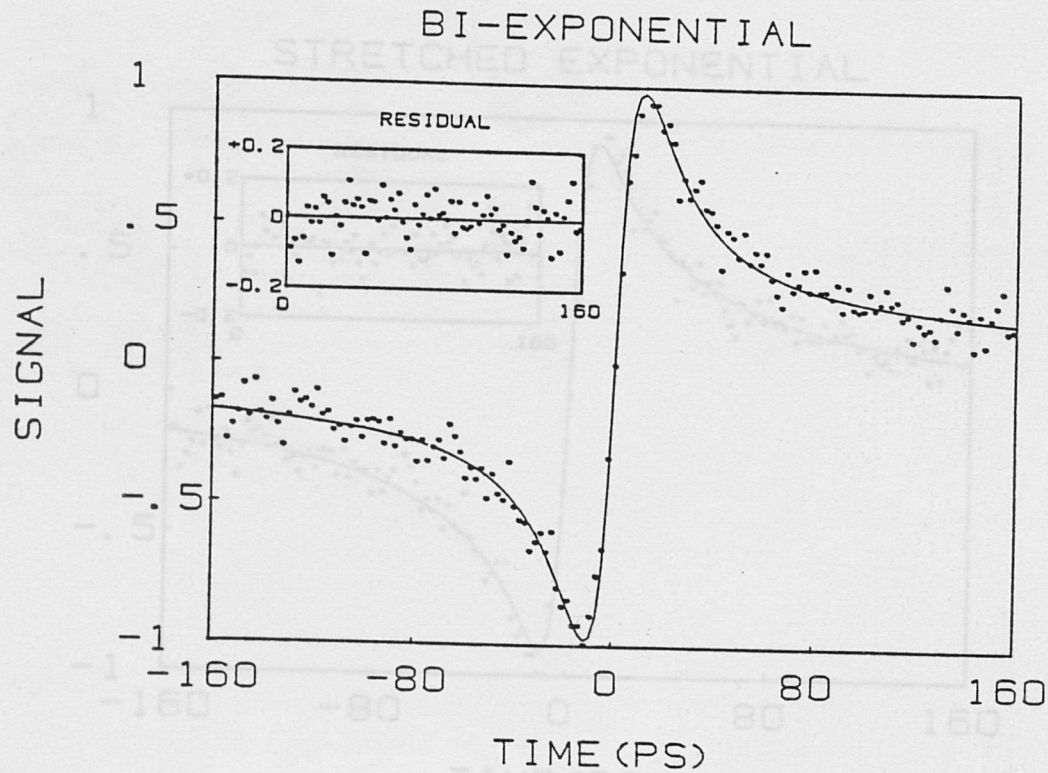

Figure 3.7

The antisymmetrized transient bleaching signals for 20 μM DDC in 3.75% colloidal silica for magic angle configuration. Solid curve is the convolution of the pulse autocorrelation with an optimized antisymmetrized biexponential function. $R_i(t) = 0.759 \exp(-t/19.02 \text{ ps}) + 0.241 \exp(-t/166.4 \text{ ps})$, $\chi^2 = 3.36 \times 10^{-3}$ Inset is a residual plot between 0 and +160 ps.

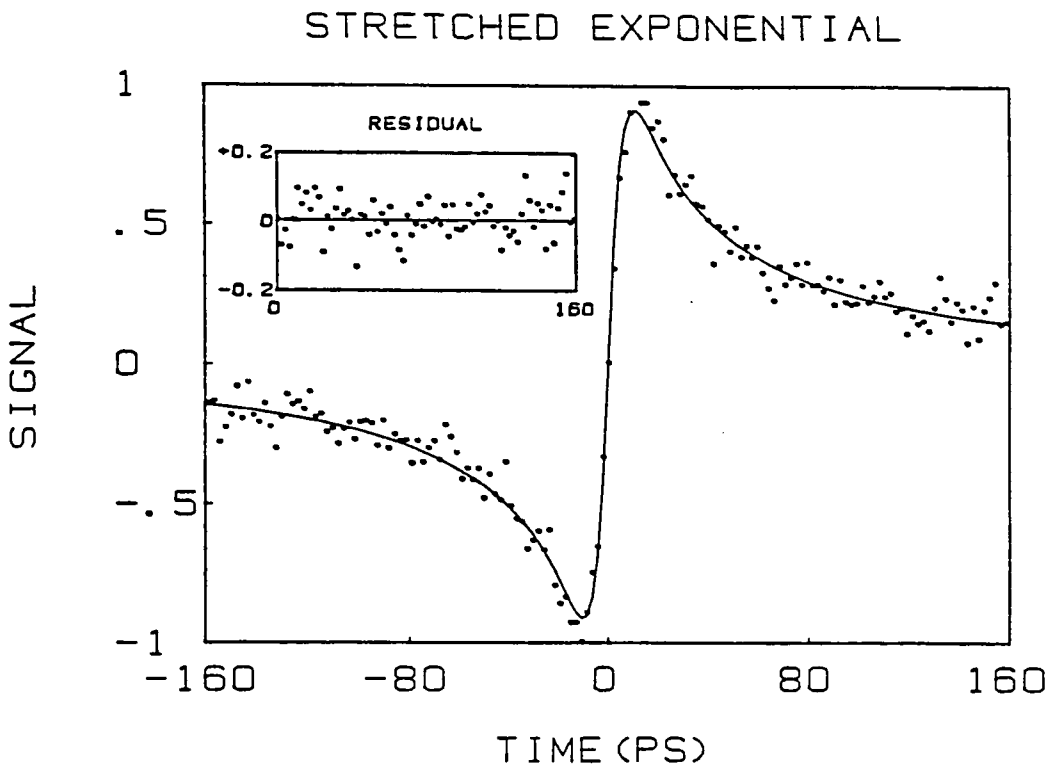

Figure 3.8

The antisymmetrized transient bleaching signals for 20 μM DDC in 3.75% colloidal silica for magic angle configuration. Solid curve is the convolution of the pulse autocorrelation with an optimized antisymmetrized stretched exponential function. $R_i(t) = \exp[-(t/15.6\ ps)^{0.46}]$, $\chi^2 = 3.359 \times 10^{-3}$. Inset is a residual plot between 0 and +160 ps.

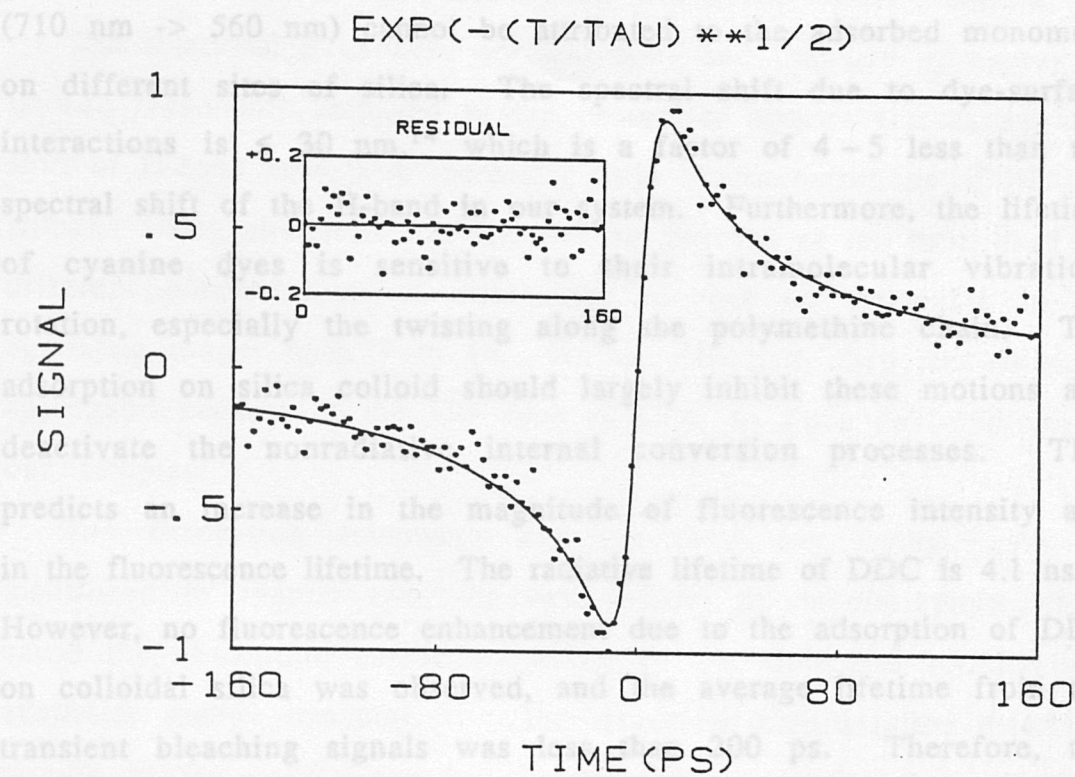

Figure 3.9

The antisymmetrized transient bleaching signals for 20 μM DDC in 3.75% colloidal silica for magic angle configuration. Solid curve is the convolution of the pulse autocorrelation with an optimized antisymmetrized function $R_i(t) = \exp[-(t/21.1\ ps)^{1/2}]$, $\chi^2 = 3.39 \times 10^{-3}$. Inset is a residual plot between 0 and +160 ps.

CHAPTER IV
DISCUSSION

The pH experiments and the ultracentrifuge results are consistent with aggregates adsorbed on silica particles. The large spectral shifts (710 nm -> 560 nm) cannot be attributed to the adsorbed monomers on different sites of silica. The spectral shift due to dye-surface interactions is ≤ 30 nm,[14] which is a factor of 4 – 5 less than the spectral shift of the H-band in our system. Furthermore, the lifetime of cyanine dyes is sensitive to their intramolecular vibration, rotation, especially the twisting along the polymethine chain. The adsorption on silica colloid should largely inhibit these motions and deactivate the nonradiative internal conversion processes. This predicts an increase in the magnitude of fluorescence intensity and in the fluorescence lifetime. The radiative lifetime of DDC is 4.1 ns.[47] However, no fluorescence enhancement due to the adsorption of DDC on colloidal silica was observed, and the average lifetime from the transient bleaching signals was less than 200 ps. Therefore, the strong dipolar coupling in H-aggregates is the most reasonable explanation to such a large spectral shift.

The weak fluorescence is well predicted by exciton theory for molecular aggregates. Because of the dipolar interaction between molecules, the excited state of the monomer will be spread out upon N-fold aggregation into an N-fold band of levels. Assuming the intrinsic rate of intersystem crossing is little affected in the monomer

upon aggregation, the spreading out of the singlet levels can be expected to enhance the rate of intersystem crossing for the aggregate. For H-aggregates, only the highest level can absorb such that high intersystem crossing probability will eliminate the internal conversion to the lowest excited state where fluorescence occurs.

The relationship between spectral shift and the size of aggregates is also reasonably reflected in the absorption spectra (increasing blue shift of H-band head with increasing ratio of concentrations of DDC to silica). Using equations 1.2, 1.4 and the position of the band head for different concentration of silica, the number of molecules in the aggregate ranges from 3 to 16. As we expected, they are all small aggregates because of the low ratio of DDC to silica concentration in our samples.

The absorption anisotropy did not show any decay. As we mentioned in chapter two, the two sources of depolarization which cause the absorption anisotropy to decay are molecular rotation and excitation energy transport. For molecular rotations, the rotational motion of the colloid can be calculated by using the Debye-Stokes-Einstein formula,[35] $\tau_{rot} = \eta V_{hyd}/k_B T$, where V_{hyd} is the volume of a sphere rotating in a liquid with viscosity η, k_B is the Boltzmann constant and T is the absolute temperature. We estimate that the rotational time of a 40-Å-diameter colloid in water at room temperature is about 7 ns. This is unimportant on the time scale to effect the anisotropy decay. The absence of faster rotation effects in the anisotropy decay in DDC molecules is another demonstration that the DDC molecules were adsorbed on the surface of colloidal silica

with fixed orientations, and were not free to rotate as in solution. The constant anisotropy in H-aggregates of DDC on colloidal silica also reflects the persistence of the coherence of the excitons. Hence the excitation in H-aggregate should be delocalized within the whole aggregate and decay exponentially (coherent exciton). We attribute the persistence of the coherence to the fact that electronic coupling between the molecules is stronger than exciton-phonon interactions which cause the excitons to become localized and to hop from molecule to molecule.

Nevertheless, the non-exponential decay really appeared in the magic angle signals. To confirm the absence of singlet-singlet exciton annihilation or other intensity-sensitive effects, we performed an intensity study by measuring the sample transmission as a function of the beam intensity. No reduction in transmission was noticed as the intensity was increased from 6 to 22 mW (typical intensities of pump beam). Hence, there is no evidence for multiphoton processes in these experiments.[49] A further check of the transient bleaching signals for different pump intensities did not show any different decay behavior. Therefore, the non-exponential decay cannot be attributed to singlet-singlet exciton annihilation.[45]

A plausible explanation for the non-exponential decay of the signal is a distribution of aggregates with different excited-state relaxation times. Bird and coworkers showed that the H-band consists of overlapping transitions.[11] For example, the H-band in the spectrum of 3,3' - bis(β - carboxyethyl)- 5,5' - dichloro - 9 - methyl - thiacarbocyanine in aqueous solution at 5°C can be resolved into

several peaks corresponding to absorption of dimer (507nm), trimers (487nm), and tetramers (477nm). Therefore, the overlapping transitions in H-band for a number of different aggregates gives rise to the inhomogeneous line broadening in our system. Since the selective excitation of individual aggregates is prohibited in this case, no apparent change in the transient bleaching signal was found for different excitation wavelengths.

The signal can be fitted well to a stretched exponential function which can be related to a distribution of exponential decays. The best stretched exponential fit in our system corresponds to $\alpha \approx 1/2$,

$$S(t) \approx \exp(-(t/\tau_p)^{1/2}) \quad . \tag{4.1}$$

If we consider there is a distribution of aggregates with different exciton lifetimes, then S(t) can be expressed as

$$\begin{aligned} S(t) &= \exp(-(t/\tau_p)^{1/2}) \\ &= \int_0^\infty F(k)\exp(-kt)dk \quad . \end{aligned} \tag{4.2}$$

The corresponding distribution of exponential rate constants F(k) is given by the inverse Laplace transform:

$$\begin{aligned} F(k) &= (2\pi i)^{-1}\int_{-i\infty}^{i\infty} S(t)\exp(kt)\ dt \\ &= F(k_o)[(k/k_o)\exp(k_o/k-1)]^{-3/2} \end{aligned} \tag{4.3}$$

where $k_o = 1/6\tau_p$ is the value of k for which F(k) peaks: hence k_o is the most probable rate constant of the distribution. The most probable life time of the aggregates can be calculated from $\tau_o = 1/k_o$. We get τ_o = 120-130 ps in our system. We were unable to obtain measurements of the excited-state lifetime of the dimer to compare with τ_o. Attempts to obtain its lifetime in water using picosecond transient photobleaching failed because of extensive photo-degradation during the measurement.

CHAPTER V

CONCLUSION

This study has revealed that 1) the formation of H-aggregates of DDC adsorbed on silica particles is confirmed, 2) the electronic excitation transport in H-aggregates of DDC adsorbed on silica particles corresponds to a coherent exciton mechanism, 3) the nonexponential transient bleaching signals can be rationalized in terms of a distribution of aggregates with different exciton lifetimes. However, the inability to selectively excite aggregate transitions and probe size effects in the excitonic properties of the aggregates is linked to spectral broadening due to dye-surface interactions and vibrations. We hope to resolve the individual aggregate transitions in future experiments by performing measurements at lower temperatures.

According to the exciton model for cyanine aggregates, major differences in the spectral properties of H-aggregates of DDC and J-aggregates of PIC are determined by the angle between the transition moments of the molecules and the axis of the aggregate. Thus, it is not surprising that both systems exhibit qualitatively similar decays. However, the pathways for electronic relaxation in these systems are not the same. Clearly, since no fluorescence is observed, electronic relaxation in an H-aggregate must largely involve nonradiative processes. In contrast, electronic relaxation in an J-aggregate involves mainly radiative processes, which is

evidenced by the intense fluorescence band. In the future, we hope to coadsorb PIC-aggregates with DDC-aggregates to simulate energy transfer between clusters of chromophores in the light-harvesting processes of the photosynthetic system. Because of the spectral overlap between the absorption band of DDC-aggregates and the emission band of PIC-aggregates, we expect to see the electronic energy transfer between the aggregates.

Although most of the results are consistent with coherence exciton, we cannot completely rule out incoherent energy transport processes that occur in less than 10 ps. To confirm this, improvements of the apparatus are necessary. Efforts are presently underway in our laboratory to establish shorter femtosecond-wide, variable wavelength pump and probe pulses to address these questions.

REFERENCES

1. Shapiro, S. L. *Ultrashort Light Pulses* (Springer, Berlin, 1977).

2. Fleming, G. R. *Chemical Applications of Ultrafast Spectroscopy* (Oxford University Press, New York, 1986).

3. Gochanour, C. R.; Fayer, M. D. *J. Phys. Chem.* 1981, *85*, 1989 and references cited therein.

4. Gochanour, C. R.; Andersen, H. C.; Fayer, M. D. *J. Phys. Chem.* 1979, *70*, 4254.

5. Anfinrud, P. A.; Causgrove, T. P. ; Struve, W. S. *J. Phys. Chem.* 1986, *90*, 5887.

6. Liang, Y.; Ponte Goncalves, A. M. *J. Phys. Chem.* 1985, *89*, 3290.

7. Turro, N. J. *Modern Molecular Photochemistry* (Benjamin/ Cummings, New York, 1978).(Benjamin/Cummings, New York, 1978).

8. Pearlstein, R. M. *Photosynthesis: Energy Conversion by Plants and Bacteria, Vol. 1* (Academic Press, New York, 1982).

9. P. Kafalas, J. Masters and E. Murray, *J. Appl. Phys.* 1964, *35*, 2349.

10. R. Cubeddu, R. Polloni, C. A. Sacchi and O. Svelto, *IEEE J. Quantum Electron.* QE-5 1969, 470.

11. Emerson, E. S.; Conlin, M. A. ; Rosenoff, A. E.; Norland, K. S.; Rodriguez, H.; Chin, D. ; Bird, G. R. *J. Phys. Chem.* 1967, *71*, 2396.

12. Herz, A. H.; Danner, R. P.; Janvsonis, G. A. *Photogr. Sci. Eng.* 1974, *18*, 323.

13. Cooper, W. *Chem. Phys. Lett.* 1970, *7*, 73.

14. Herz, A. H. In the *Theory of the Photographic Process*, 4th ed.; James, T. H., Ed. (MacMillan, New York, **1977**) pp. 235-250.

15. Jelley, E. E. *Nature* (London) **1937**, *139*, 631.

16. McRae, E. G.; Kasha, M. *J. Chem. Phys.*, **1958**, *28*, 721.

17. Herz, A. H. In the *Theory of the Photographic Process*, 4th ed.; James, T. H., Ed. (MacMillan, New York, **1977**) pp. 194-195.

18. West, W.; Pearce, S. *J. Phys. Chem.* **1965**, *69*,1894.

19. Mattoon, R. W. *J. Chem. Phys.* **1944**, *12*, 268.

20. Grover, M.; Silbey R. *J. Chem. Phys.* **1971**, *54*, 4843.

21. Davydov, A. S. *Theory of Molecular Excitons* (McGraw-Hill, New York, **1962**).

22. Knox, R. S. *Top. Photosynth.* **1977**, *2*, 55-97.

23. Forster, T. In *Modern Quantum Chemistry*; Sinanoglu, D. Ed. (Academic Press, New York, **1965**), Part 3, pp. 93-137.

24. McRae, E. G. *Australian J. Chem.* **1961**, *14*, 354.

25. Juzeliunas, G. Z. *Phys. D. Atomic, Molecules and Clusters* **1988**, *8*, 379.

26. Pearlstein, R. M.; Lindenberg, K.; Hemenger, R. P. In *Excited States of Biological Molecules*; Birks, J. B. Ed. (Wiley, New York) pp. 591-600.

27. Quitevis, E. L.; Horng, M.; Chen, S. *J. Phy. Chem.* **1988**, *92*, 256.

28. Weitz, D. A.; Garoff, S.; Gersten, J. I.; Nitzan, A. *J. Chem. Phys* **1983**, *78*, 5324.

29. Bard, A. J. *J. Phys. Chem.* **1982**, *86*, 172.

30. Iler, R. K. *The Chemistry of Silica*, 2nd ed. (Wiley, New York, **1979**).

31. Wheeler, J.; Thomas, J. K. *Inorganic Reactions in Organized Media*; Holt, S. L., Ed. (American Chemical Society, Washington, D. C., **1982**) ACS Symp. Ser. No. 177, pp. 98-111.

32. Laane, C.; Willner, I.; Otvos, J. W.; Calvin, M. *Proc. Natl. Acad. Sci.* USA, **1981**, *78*, 5928.

33. Rehm, D.; Eisenthal, K. B. *Chem. Phys. Lett.* **1971**, *9*, 387.

34. Bado, P.; Wilson, S. B.; Wilson, K. R. *Rev. Sci. Inst.* **1982**, *53*, 706.

35. Quitevis, E. L.; Casey, K. G.; Sinor, T. W. *Chem. Phys. Lett.* **1986**, *132*, 77.

36. Gillbro, T.; Sandstrom, A., Sundstrom, V.; Holzwarth, A. R. *FEBS Lett.* **1983**, *162*, 64.

37. Causgrove, T. P.; Yang, S.; Struve, W. S. *J. Phys. Chem.* **1988**, *92*, 6121.

38. Shank, C. V.; Auston, D. H. *Phys. Rev. Lett.* **1975**, *34*, 479.

39. Jena, A.; Lessing, H. E. *Appl. Phys.* **1979**, *19*, 131.

40. Engh, R. A.; Petrich, J. W.; Fleming, G. R. *J. Phys. Chem.* **1985**, *89*, 618.

41. Alivisatos, A. P.; Arndt, M. F.; Efrima, S.; Waldeck, D. H.; Harris, C. B. *J. Chem. Phys.* **1987**, *86*, 6540.

42. Richert, R.; Bassler, H. *J. Chem. Phys.* **1986**, *84*, 3567.

43. Bevington, P. R. *Data Reduction and Error Analysis for the Physical Sciences* (McGraw-Hill, New York, **1969**).

44. West, W.; Carroll, B. H.; Whitcomb, D. L. *J. Phys. Chem.* **1952**, *56*, 1054.

45. Doukas, A. G.; Stefancic, V.; Buchert, J.; Alfano, R. R.; Zilinskas, B. A. *Photochem. Photobiol.* **1981**, *34*, 505.

46. Brumbaugh, D. V.; Muenter, A. A. *J. Lumi.* **1984**, *32*, 783.

47. Dempster, D. N.; Morrow, T.; Rankin, R.; Thompson, G. F. *Chim. Phys. Lett.* **1973**, *18*, 488.

48. Philpott, B. R. *J. Chem. Phys.* **1975**, *63*, 485.

49. Kopainsky, B.; Kaiser, W. *Chem. Phys. Lett.* **1982**, *88*, 357.

50. Kazuhiko Kinosita, Jr.; Suguru Kawato; Akira Ikegami *J. Biochem.* **1977**, *20*, 289.

51. Doba, T.; Ingold, K. U.; Siebrand, W.; Wildmann, T. A. *Chem. Phys. Lett.* **1985**, *115*, 51.

PERMISSION TO COPY

In presenting this thesis in partial fulfillment of the requirements for a master's degree at Texas Tech University, I agree that the Library and my major department shall make it freely available for research purposes. Permission to copy this thesis for scholarly purposes may be granted by the Director of the Library or my major professor. It is understood that any copying or publication of this thesis for financial gain shall not be allowed without my further written permission and that any user may be liable for copyright infringement.

Disagree (Permission not granted)	Agree (Permission granted)
	Sung-yong Chen
Student's signature	Student's signature
	11-28-88
Date	Date